Compressive damage of composite structures using 3D failure criteria and 2D higher-order structural theories

Compressive damage of composite structures using 3D failure criteria and 2D higher-order structural theories

M. Petrolo*, E. Tortorelli†, S. Saputo‡

MUL^2 Lab, Department of Mechanical and Aerospace Engineering,
Politecnico di Torino, Corso Duca degli Abruzzi 24, 10129 Torino, Italy

Revised version of Manuscript Number 258917738

Author for correspondence:
Marco Petrolo
MUL^2 Lab, Department of Mechanical and Aerospace Engineering,
Politecnico di Torino,
Corso Duca degli Abruzzi 24,
10129 Torino, Italy,
tel: +39 011 090 6845,
e-mail: marco.petrolo@polito.it

*Associate Professor. E-mail: marco.petrolo@polito.it
†PhD Student. E-mail: elisa.tortorelli@polito.it
‡Research Assistant. E-mail: salvatore.saputo@polito.it

Abstract: *This paper analyzes the compressive damage behavior of composite plates using 2D structural theories and 3D failure criteria. The proposed approach integrates the Carrera Unified Formulation (CUF), 3D Hashin failure model for fibers, and Puck's matrix compression criterion. It features advanced modeling of the fracture plane orientation and progressive material degradation. The structural modeling is layer-wise (LW) and enhances computational efficiency while maintaining high accuracy compared to traditional finite element approaches. Verification and validation are carried out on single-element tests, compact compression tests, and open-hole compression tests, with the results demonstrating strong agreement with experimental data and existing numerical models. The study highlights the benefits of using higher-order 2D structural theories instead of refined meshes to capture the complex failure mechanisms of fiber-reinforced composites under compression.*

Keywords: Composites; Damage; Hashin; Puck; CUF, FEM.

1 Introduction

Fiber-reinforced composite materials are commonly used in various engineering applications, including aerospace industry ones, due to their good specific strength and stiffness, as discussed in [1]. The failure analysis of composites is still challenging due to multiple failure modes. The compressive failure mechanism is particularly challenging due to the interplay of failure modes such as the fiber micro-buckling, kinking, and matrix shear failure [2, 3, 4]. Another complicating factor is the presence of manufacturing defects, including fiber misalignment and micro-structural voids, which can significantly impact material performance [5, 6]. Understanding and accurately modeling these failure mechanisms are crucial for composite structure's reliable and efficient design [7].

Damage modeling approaches for fiber-reinforced composites belong to discrete damage models (DDM) and continuum damage models (CDM). DDM explicitly models the geometry of cracks within a structure. DDM, including the extended finite element method (X-FEM) and cohesive zone modeling (CZM), provides high-fidelity predictions of crack initiation and propagation, see [8], but requires significant computational resources. CDM, conversely, has lower computational costs [9] and models the damage evolution through degradation parameters within the constitutive equations. While CDM has been widely applied to tensile damage analysis, its extension to compressive damage remains relatively under-explored. Some examples of application are the analysis of an open-hole composite laminate [10] and the notched omega stiffened composite panels [11].

In CDM, the material degradation laws exploit failure criteria to predict damage initiation, progressive failure, and ultimate failure strengths. Different criteria are available, e.g., Hashin, Puck, Hoffman, and Tsai-Wu [12, 13, 14, 15].

An example of a modeling approach for the nonlinear behavior induced by damage is the CODAM, initially developed for macroscopic sub-laminate level modeling of composites as discussed in [16]. CODAM provides intralaminar damage based on continuum damage mechanics and uses failure criteria for fibers and matrices. The second-generation model, known as CODAM2, translates the sub-laminate strain-softening behavior into equivalent stress-strain responses along the principal ply directions [17], and it was implemented in various

finite element commercial software as LS-DYNA [18, 19].

The progressive damage analysis of composite structures may require a high computational cost due to the refined meshes needed to obtain an accurate stress field. Different techniques have been proposed in the literature to overcome this problem, such as solid/shell coupling, where the solid elements are used only in the critical region [20], and the global/local method as in [21].

The present work aims to reduce the computational cost of progressive failure analysis of composites under compression using 2D structural theories. In the previous works by the authors, the nonlinear material behavior of composite structures was described via CODAM2 for both traction [22] and compression [23]. The present work's novelty stems from using a different damage model based on Hashin 3D and Puck failure criteria for matrix compression [24, 25]. The selection of the Puck criterion for the matrix leads to a more accurate matrix compression failure as it features inclined fracture mechanisms as observed in experimental studies [26, 27, 28].

The computational efficiency improvement is due to using Carrera Unified Formulation (CUF) for the structural modeling [29]. CUF enables the development of higher-order 1D and 2D theories, wherein the accuracy is augmented through the utilization of cross-section and thickness expansion functions instead of mesh refinement. CUF efficiency reduces computational cost when compared with standard solid element FE analyses. Others examples of CUF models applied for progressive analysis can be found in [30], where the micromechanical framework exploits a class of refined 1D models or for the evaluation a model's performance based on the failure index in [31]. In this work, higher-order 2D theories are employed. The layer-wise (LW) approach is used to model the though-the-thickness behavior of plates [32].

This paper is organized as follows: Section 2 presents CUF and the FE formulation; Section 3 presents the damage model and the various failure criteria employed for both fiber and matrix. Numerical results are shown in Section 4 and key conclusions in Section 5.

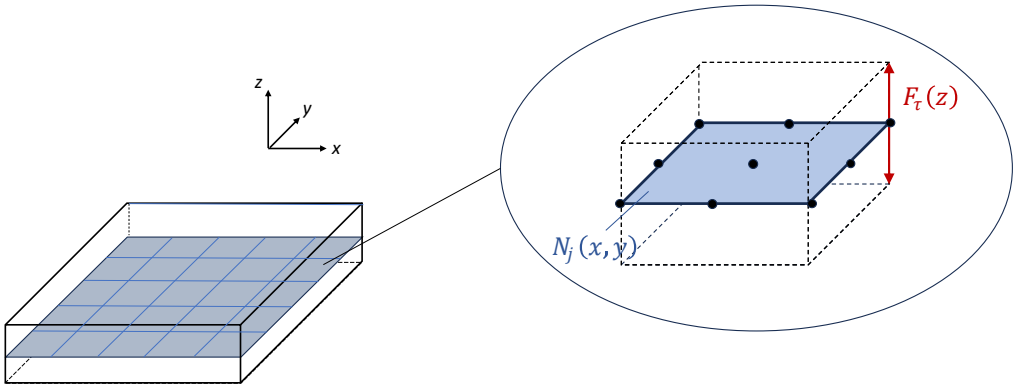

Figure 1: 2D-CUF model with Q9 elements

2 Structural theories and finite element formulation

According to CUF for 2D theories [29], and using the reference frame shown in 1, the 3D displacement field, $\boldsymbol{u}(x, y, z)$, can be expressed as a product between in-plane shape functions, N_i(x,y) and expansion functions acting along the thickness, F_τ(z),

$$\boldsymbol{u}(x, y, z) = F_\tau(z) N_i(x, y) \boldsymbol{u}_{\tau i}, \qquad \tau = 1, ..., M \qquad i = 1, ..., p \tag{1}$$

F_τ(z) is the expansion function modeling the displacement filed along the thickness and having "M" terms. $\boldsymbol{u}_{\tau i}$ is the nodal unknown vector. N_i(x,y) are the 2D shape functions, and p is the number of nodes of each element. The results of this work are obtained using standard Q4 and Q9 elements. The structural theories exploit Lagrange polynomials as expansion functions through the layer thickness [32] and leading to a layer-wise (LW) description of the displacement field,

$$\boldsymbol{u}^k(x, y, \zeta^k) = F_\tau^k(\zeta^k) \boldsymbol{u}_\tau^k(x, y), \qquad \tau = 1, ..., M \tag{2}$$

k is the ply index and ζ^k spans the ply thickness, [-1,1]. The current work uses first- (LE1), second- (LE2), and third-order (LE3) polynomials. The stress and strain components are grouped as follows:

$$\begin{aligned} \boldsymbol{\sigma} &= \{\sigma_{xx}, \sigma_{yy}, \sigma_{zz}, \sigma_{xy}, \sigma_{xx}, \sigma_{yz}\} \\ \boldsymbol{\epsilon} &= \{\epsilon_{xx}, \epsilon_{yy}, \epsilon_{zz}, \epsilon_{xy}, \epsilon_{xz}, \epsilon_{yz}\} \end{aligned} \tag{3}$$

By considering the geometrically linear assumptions, the linear strain-displacement relation is

$$\boldsymbol{\epsilon} = \mathbf{B}\boldsymbol{u} \tag{4}$$

where $\boldsymbol{u}$ is the displacement vector and $\mathbf{B}$ is the linear differential operator given by

$$\boldsymbol{b_l} = \begin{bmatrix} \partial_x & 0 & 0 \\ 0 & \partial_y & 0 \\ 0 & 0 & \partial_z \\ \partial_y & \partial_x & 0 \\ \partial_z & 0 & \partial_x \\ 0 & \partial_z & \partial_y \end{bmatrix} \tag{5}$$

The constitutive relation in the damage state is obtained through the secant material stiffness matrix, $\mathbf{C}^{sec}$,

$$\boldsymbol{\sigma} = \mathbf{C}^{sec}\epsilon \tag{6}$$

As commonly implemented for this class of problems, explicit time integration techniques and the central difference scheme are employed to solve equations given by the semi-discrete balance of momentum,

$$\boldsymbol{M}\ddot{\boldsymbol{u}} = \boldsymbol{F}_{ext} - \boldsymbol{F}_{int} \tag{7}$$

where $\boldsymbol{M}$ is the mass matrix, $\ddot{\boldsymbol{u}}$ is the acceleration vector, and $\boldsymbol{F}_{ext}$, $\boldsymbol{F}_{int}$ the external and internal force vectors, respectively. More details about the explicit nonlinear formulation in CUF can be found in [22].

3 Damage model

The current work adopts 3D Hashin criteria for matrix, fiber tension, and compression. For matrix compression, the Puck criterion was considered according to the works of Davila et al. [28] and Lapczyk et al. [33]. The failure index referring to the fiber damage initiation for compression, F_{fc}, in Hashin 3D is given by

$$F_{fc} = \left(\frac{\sigma_{11}}{X_C}\right)^2 \tag{8}$$

X_C is the fiber compressive strength. The matrix damage initiation along the transverse direction occurs when $\mathrm{F}_{mc} \geq 1$, where the Puck failure criteria is given by

$$F_{mc} = \left(\frac{\sigma_{nt}}{S_{23}^A - \eta_{nt}\sigma_{nn}}\right)^2 + \left(\frac{\sigma_{nl}}{S_{12} - \eta_{nl}\sigma_{nn}}\right)^2 \tag{9}$$

The internal material friction is characterized by the coefficients η_{nl} and η_{nt} based on the Mohr-Coulomb failure theory [34]; σ_{nn}, σ_{nl} and σ_{nt} are stresses along the normal, longitudinal shear and transverse shear directions of the fracture plane, respectively; S_{12} is the in-plane shear strength and S_{23}^A is the transverse shear strength in the fracture plane. The terms employed in the failure criterion are given by

$$\begin{aligned}
\sigma_{nn} &= \sigma_{22}\cos^2\theta + \sigma_{33}\sin^2\theta + 2\sigma_{23}\cos\theta\sin\theta \\
\sigma_{nl} &= \sigma_{12}\cos\theta + \sigma_{13}\sin\theta \\
\sigma_{nt} &= -\sigma_{22}\cos\theta\sin\theta + \sigma_{33}\cos\theta\sin\theta + 2\sigma_{23}(2\cos^2\theta - 1) \\
\mu_{nt} &= \tan(2\theta - 90^\circ), \quad \frac{\mu_{nt}}{S_{23}^A} = \frac{\mu_{nl}}{S_{12}}, \quad S_{23}^A = \frac{Y_C}{2}\left(\frac{1-\sin\phi}{\cos\phi}\right), \quad \phi = 2\theta - 90^\circ
\end{aligned} \tag{10}$$

θ is the fracture angle, which is approximately 53° for a unidirectional composite under uniaxial transverse compressive load as found by Donadon et al. [35]. The Puck criterion estimates the inclination of the most probable fracture plane by calculating θ. The Simple Parabolic Interpolation Search (SPIS) is adopted in this paper as proposed in [36]. SPIS divides the overall 180° interval into 18 sub-intervals, each comprising 19 reference points, as shown in Fig. 2, to evaluate F_{mc} and, then, θ.

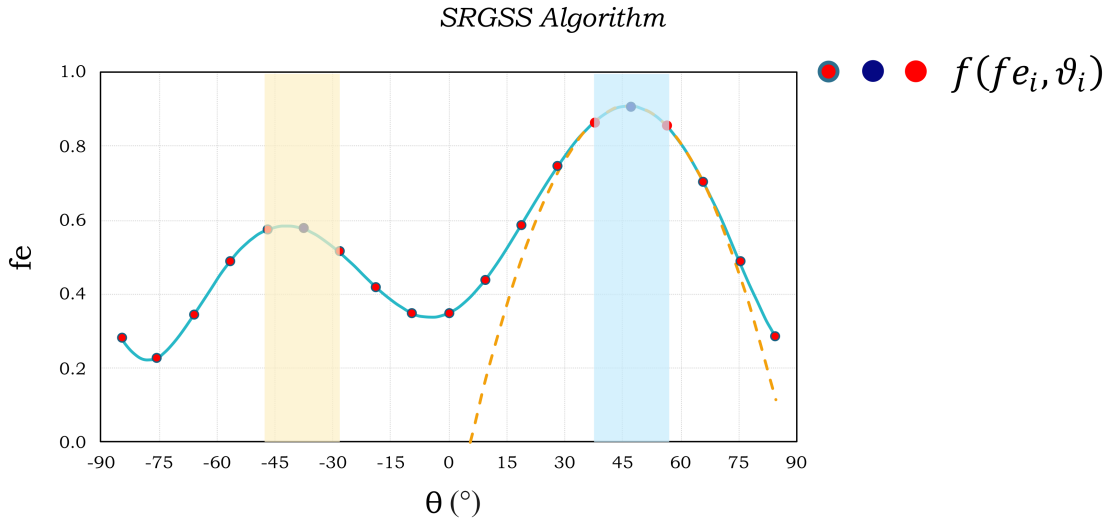

Figure 2: An example of SPIS method based on [36]

To compute the damage progression, the equivalent compressive displacements δ_{eq}^{fc} and δ_{eq}^{mc}, for fibers and matrix, are used,

$$\delta_{eq}^{fc} = l_c\langle -\epsilon_{11}\rangle \tag{11}$$

$$\delta_{eq}^{mc} = l_c\sqrt{\langle -\epsilon_{22}\rangle^2 + \langle -\epsilon_{33}\rangle^2 + \epsilon_{12}^2 + \epsilon_{23}^2 + \epsilon_{13}^2} \tag{12}$$

$\langle\cdot\rangle$ is the Mcaulay bracket, l_C is the characteristic length set equal to the cubic root of the Gauss point volume, $l_C = (V_{GP})^{1/3}$. The Gauss point volume is the portion of the element volume associated with each Gauss point. The relation between displacement and strain is given by $\delta_{eq} = l_c\epsilon_{eq}$. The corresponding equivalent stresses in the longitudinal and transverse directions are

$$\sigma_{eq}^{fc} = \frac{l_c\langle -\sigma_{11}\rangle\langle -\epsilon_{11}\rangle}{\delta_{eq}^{fc}} \tag{13}$$

$$\sigma_{eq}^{mc} = \frac{l_c(\langle -\sigma_{22}\rangle\langle -\epsilon_{22}\rangle + \langle -\sigma_{33}\rangle\langle -\epsilon_{33}\rangle + \sigma_{12}\epsilon_{12} + \sigma_{23}\epsilon_{23} + \sigma_{13}\epsilon_{13})}{\delta_{eq}^{mc}} \tag{14}$$

The ultimate displacement at damage saturation is

$$\delta_{eq}^{u,f} = \frac{2G_f}{T} \tag{15}$$

$$\delta_{eq}^{u,m} = \frac{2G_m}{T} \tag{16}$$

G_f and G_m are the fracture energies in longitudinal and transverse directions, respectively; T is the peak value of the equivalent transverse stress when the damage occurs, T= $\sigma_{eq}^{mtc}\big|_{F_t=1}$ and T= $\sigma_{eq}^{mtc}\big|_{F_m=1}$, respectively. The damage evolution parameter, d, is

$$d = \frac{\delta_{eq}^{u}(\delta_{eq} - \delta_{eq}^{0})}{\delta_{eq}(\delta_{eq}^{u} - \delta_{eq}^{0})} \tag{17}$$

$\delta_{eq}^{0} = \delta_{eq}\big|_{F=1}$ is the equivalent displacement at the damage initiation. As discussed in [37], the constitutive elastic stress-strain relation during the damage evolution can be written as

$$\boldsymbol{\sigma} = \boldsymbol{C}^{dam}\boldsymbol{\epsilon} \tag{18}$$

where $\boldsymbol{C}^{dam}$ is the stiffness matrix in the damage state. It can be computed using Δ,

$$\Delta = 1-(1-d_f)(1-d_m)\nu_{12}\nu_{21}-(1-d_m)\nu_{23}\nu_{32}-(1-d_f)\nu_{13}\nu_{31}-2(1-d_f)(1-d_m)\nu_{21}\nu_{32}\nu_{13} \tag{19}$$

The damage parameters, d_f and d_m, are

$$d_f = 1 - (1 - d_{ft})(1 - d_{fc}) \tag{20}$$

$$d_m = 1 - (1 - d_{mt})(1 - d_{fc}) \tag{21}$$

d_{ft} and d_{mt} refer to fiber and matrix traction, d_{fc} and d_{mc} to fiber and matrix compression. The damage matrix is

$$\boldsymbol{C}^{dam} = \frac{1}{\Delta}\begin{bmatrix} C_{11} & C_{12} & C_{13} & 0 & 0 & 0 \\ C_{21} & C_{22} & C_{23} & 0 & 0 & 0 \\ C_{31} & C_{32} & C_{33} & 0 & 0 & 0 \\ 0 & 0 & 0 & C_{44} & 0 & 0 \\ 0 & 0 & 0 & 0 & C_{55} & 0 \\ 0 & 0 & 0 & 0 & 0 & C_{66} \end{bmatrix} \tag{22}$$

where the matrix components are defined as follows

$$\begin{aligned} C_{11} &= [1-(1-d_m)\nu_{23}\nu_{32}](1-d_f)E_1 \qquad C_{12} = (1-d_f)(1-d_m)(\nu_{21}+\nu_{23}\nu_{31})E_1 \\ C_{22} &= [1-(1-d_f)\nu_{31}\nu_{13}](1-d_m)E_2 \qquad C_{13} = (1-d_f)(\nu_{31}+(1-d_m)\nu_{21}\nu_{32})E_1 \\ C_{33} &= [1-(1-d_f)(1-d_m)\nu_{21}\nu_{12}]E_3 \qquad C_{23} = (1-d_m)(\nu_{32}+(1-d_f)\nu_{12}\nu_{31})E_2 \\ C_{44} &= \Delta(1-d_f)(1-d_m)G_{12} \qquad\qquad C_{55} = \Delta G_{23} \\ C_{66} &= \Delta G_{13} \end{aligned} \tag{23}$$

More details on the implementation of damage models in CUF can be found in [22, 23].

Bi-linear constitutive models with a linear post-peak softening response often struggle to

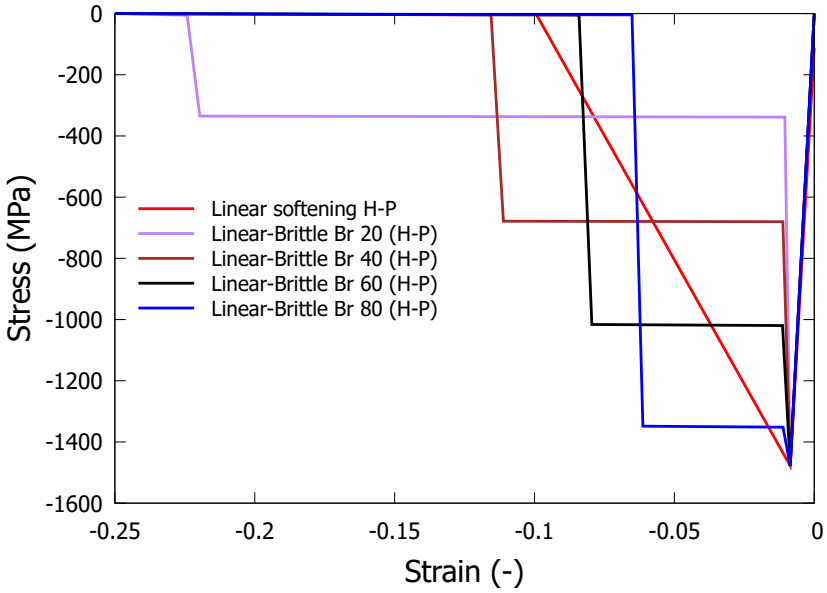

Figure 3: Family of softening curves

accurately capture the complex behavior of fiber failure under compressive loads. One of the main challenges is the instability that occurs during the initiation and propagation of fiber damage, leading to micro buckling and the formation of kink bands. These failure mechanisms result in a sharp reduction in the load-carrying capacity of the material, followed by a stress plateau. A simple linear softening approach cannot effectively replicate this response as it does not account for the rapid loss of strength and subsequent stabilization phase, as explained in [38]. Alternative softening curves have been introduced to enhance the predictive accuracy of the material model [39]. These modifications involve refining the damage evolution law, incorporating a 'linear-brittle' softening curve that better represents the sharp stress drop and the following plateau. This approach ensures a more realistic depiction of compressive failure progression. A key aspect of this enhanced modeling is the residual plateau stress, which is defined as a fraction of the peak stress. By adjusting this percentage, a family of softening curves can be generated, capturing variations in compressive failure behavior. Importantly, the fracture energy associated with fiber failure remains constant across these curves, ensuring consistency in energy dissipation during damage evolution. An example of a family of softening curves using the H-P failure criteria is shown in Fig. 3.

Table 1: Material properties of IM7/8552

E_1 (GPa)	E_2 (GPa)	E_3 (GPa)	G_{12} (GPa)	G_{13} (GPa)	G_{23} (GPa)	ν_{12}	ν_{13}	ν_{23}
150.0	11.0	11.0	5.8	5.8	2.9	0.34	0.34	0.48
X_T (MPa)	X_C (MPa)	Y_T (MPa)	Y_C (MPa)	S_{12} (MPa)	G_1^T (kJ/m^2)	G_2^T (kJ/m^2)	G_1^C (kJ/m^2)	G_2^C (kJ/m^2)
2560	1690	73	250	90	120	2.6	80.0	4.2

4 Numerical results

The numerical simulations developed using Hashin 3D and Puck criteria for compression—referred to as H-P—are compared with those from other modeling approaches and experiments. The aim is to verify, validate, and assess the new approach, considering accuracy and numerical efficiency. The material properties used for all cases are listed in Table 1.

4.1 Single element

The first case considers a single element of 1 mm × 1 mm. The material is IM7/8552 carbon fiber reinforced polymer (CFRP) with a ply thickness of 0.125 mm. The CUF structural model adopted is one four-node Q4 element as in-plane discretization with a linear Lagrange expansion LE1 along the thickness as in the previous work based on CODAM2 [23]. Three cases are considered: the first refers to a uni-axial compression in the longitudinal direction with the fibers aligned to the y-direction (0°); the second case consists of the uni-axial compression in the transverse direction concerning the fiber (90°); the last case refers to the uni-axial compression of a single element quasi-isotropic with lamination of $[90/45/0/\text{-}45]_{2s}$. The boundary conditions and results of the analyses are shown in Fig. 4. In Fig. 4a-4b, the results are compared with those from CODAM2-CUF based on 2D Hashin [23]. In Fig. 4c, the stress-strain curve is compared with the CODAM2-CUF approach, two different damage models using LS-DYNA and ABQ-DLR-UD in ABAQUS [40]. The LS-DYNA models refer to CODAM2, implemented as MAT219, and to the Laminate-Based Composite Model, implemented as MAT81. The user-defined material model ABQ-DLR-UD in Abaqus/Explicit uses Ladeveze's coupled transverse and shear damage formulation [9]. The results show that:

1. The peak stresses predicted by the present model match the material strengths of the fiber - 1690 MPa - and matrix - 250 MPa; it also matches the value obtained by the

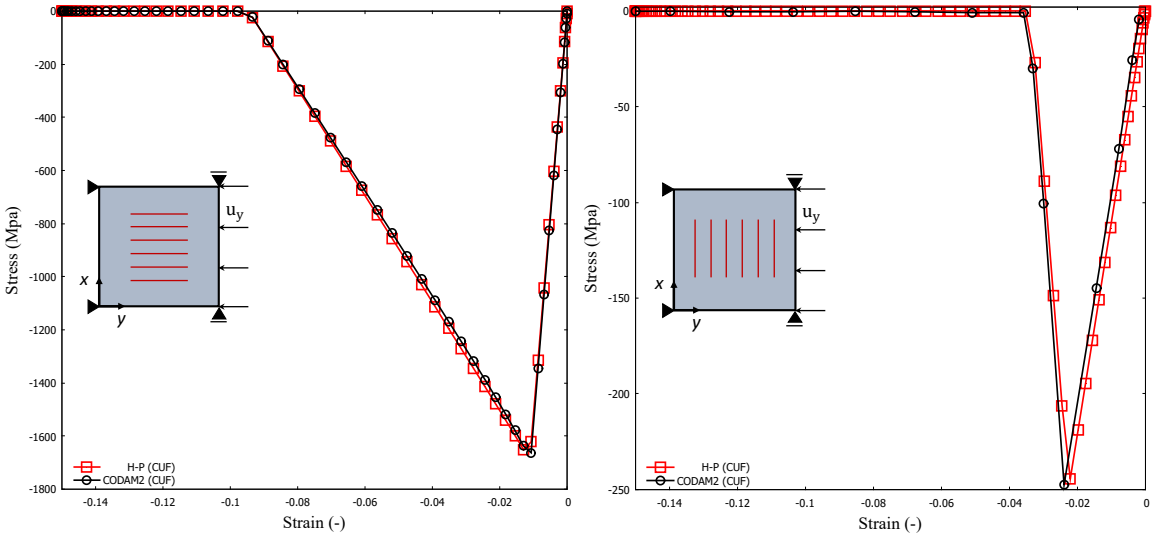

(a) Longitudinal loading (0°) (b) Transverse loading (90°)

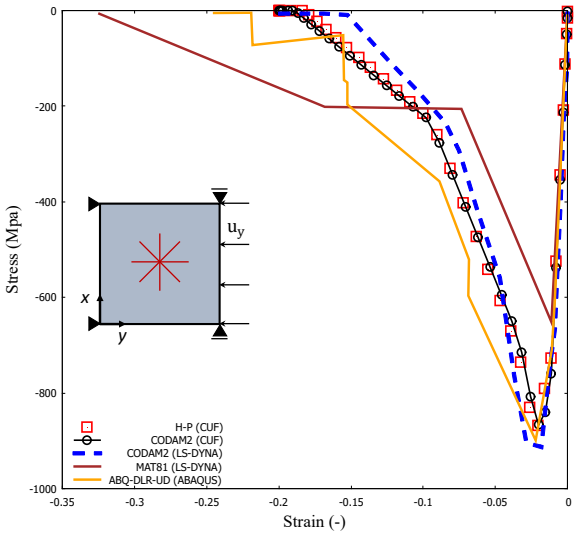

(c) Quasi-isotropic

Figure 4: Stress-strain response of the single element under uni-axial compression

Model	Elements	DOF
CUF 191Q9-LE1	191 Q9 elements in-plane and 1 LE1 per ply	82467
CUF 191Q9-LE2	191 Q9 elements in-plane and 1 LE2 per ply	162435
CUF 191Q9-LE3	191 Q9 elements in-plane and 1 LE 3 per ply	242403
MAT18 (LSDYNA)	4848 shell elements	N/A

Table 2: Number of elements and DOF in models of the CC test

CODAM2-CUF. The fracture energy matches very well too, and it is given by the area under the stress-strain curve, i.e., 80 kJ/m^2 and 4.2 kJ/m^2 in the longitudinal and transverse direction, respectively.

2. For the quasi-isotropic element, the peak matches well with all other models but MAT81, which predicts a significantly lower peak stress - around 30% lower than H-P, CODAM2, and ABQ-DLR-UD. The difference may be due to the assumption of a simplified laminate behavior in which the multilayer system is homogenized, whereas the other models consider fiber and matrix failure separately. CUF employs a combination of one Q4 and one LE1 per layer, whereas the LS-DYNA model utilizes a stacked 3D shell approach to model the single-element laminate.

4.2 Compact compression test

The second test consists of a compact compression test (CC) of quasi-isotropic $[90/45/0/\text{-}45]_{4s}$ laminate; the geometry and loads are shown in Fig. 6. This numerical case was retrieved from [41], in which the authors conducted a quasi-static fracture experimental tests; afterwards, in [40], the authors used CODAM2 and MAT81 damage models in LS-DYNA for the same case. Figure 6 also shows the 2D mesh adopted in CUF and retrieved from [23]. The mesh has 191 Q9 elements, while LE1, LE2, and LE3 expansion functions are adopted for each laminate ply along the thickness. Table 2 lists the number of elements of models used for this case. Figure 5 shows the force and Pin Opening Displacement (POD) curves. CUF models have linear softening post-peak curves. CUF models have different expansion functions along the thickness, from linear to cubic. The force-POD curves derived from experimental testing and the MAT81 damage model in LS-DYNA are also plotted. The value of peak force, the POD related to the peak force, and the corresponding error with respect to the experimental values

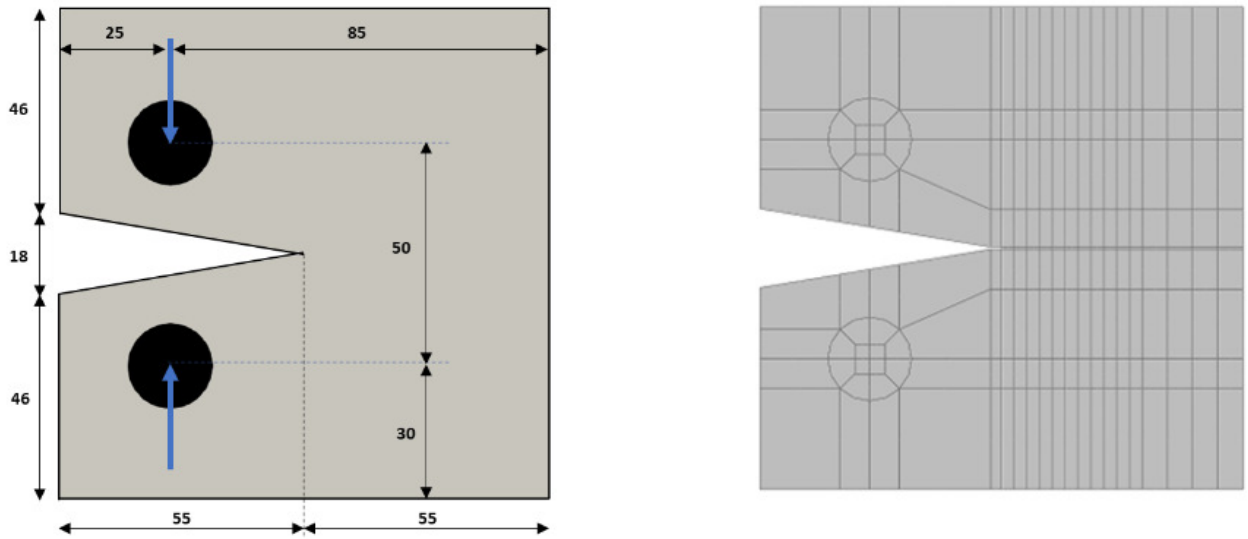

Figure 5: Geometry and in-plane discretization of the CC; dimensions are in mm and the FE mesh has 191 Q9 elements

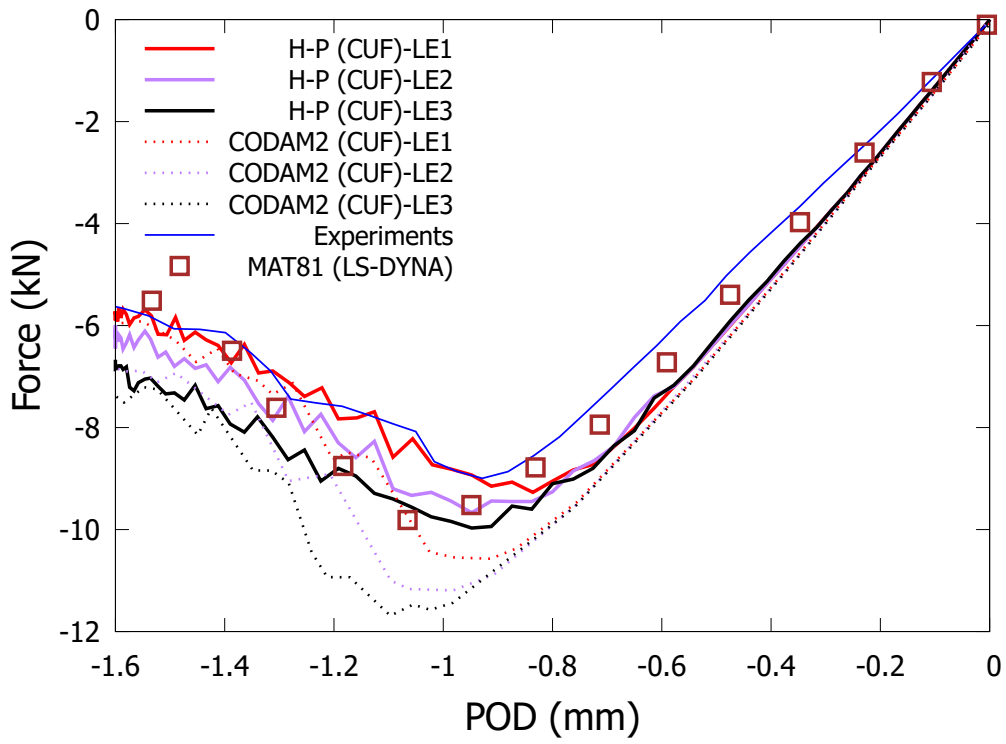

Figure 6: Force-POD curves of the CC

Approach	Peak Force (kN)	Error (%)	POD at peak force (mm)	Error (%)
Experiments	-9.092	–	0.932	–
MAT81 (LS-DYNA)	-9.912	9.0	1.005	7.8
H-P (CUF)-LE1	-9.267	1.49	0.836	-10.3
H-P (CUF)-LE2	-9.668	6.3	0.948	1.87
H-P (CUF)-LE3	-9.965	9.6	0.948	1.87
CODAM2 (CUF)-LE1	-10.671	17.4	0.887	-4.8
CODAM2 (CUF)-LE2	-11.283	24.1	0.962	3.2
CODAM2 (CUF)-LE3	-11.808	29.9	1.074	15.2

Table 3: Comparison of peak forces and POD at peak force for different approaches for the CC

are listed in Table 3. Figure 7a shows the LE1 case; the vertical lines indicate three POD values: -0.687, -0.836, and -0.985 mm. Figure 7b shows the damage progression for the three selected POD values in fiber and matrix. The results suggest that:

1. There is a good agreement between force-POD curves obtained using the H-P damage model and the experimental results.

2. The H-P damage model in the case of linear softening better matches the experimental results than CODAM2. The percentage errors for peak forces and POD at peak force are always less than 10%. Parabolic and cubic expansions improve the POD at peak forces, but some oscillations in the convergence are found concerning the peak forces. The problem considered is in-plane; therefore, LE1 can be considered enough for accurate results. Higher-order theories may play a more significant role when interlaminar effects are present, such as delamination.

3. Differences in the slope of the linear branches may be due to the inability to replicate the same boundary conditions as in the experimental real case.

4. Oscillations in the post-peak curve in the CUF approaches may be caused by the absence of numerical damping.

5. The H-P CUF approach has a lower percentage error than MAT81 with LS-DYNA. The latter is based on the homogenization of the laminate, while the former retains each ply properties through a layer-wise approach.

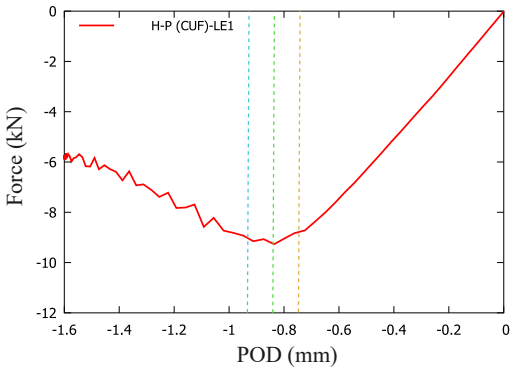

(a) Force-POD curve

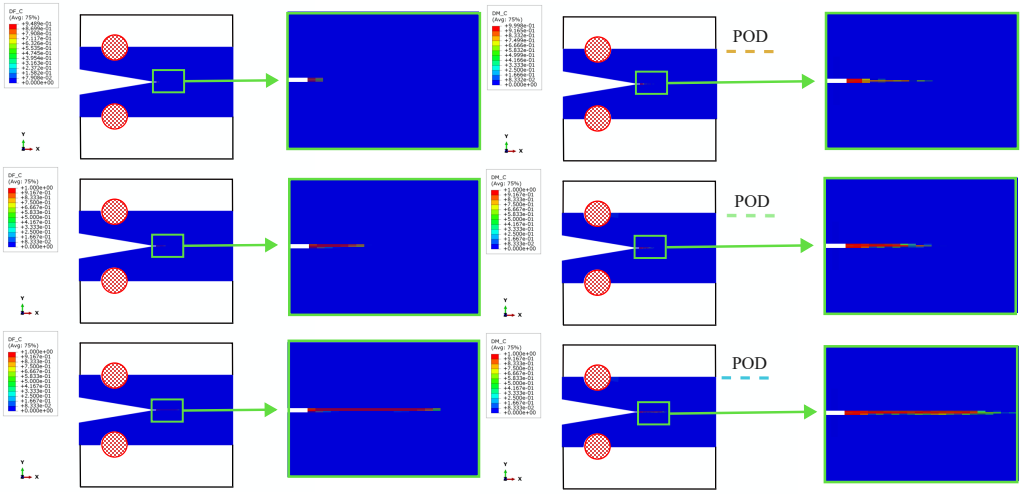

(b) Damage distributions

Figure 7: Damage progression for the H-P LE1 model at -0.687, -0.836 and -0.985 mm POD, respectively; fiber damage on the left and matrix damage on the right

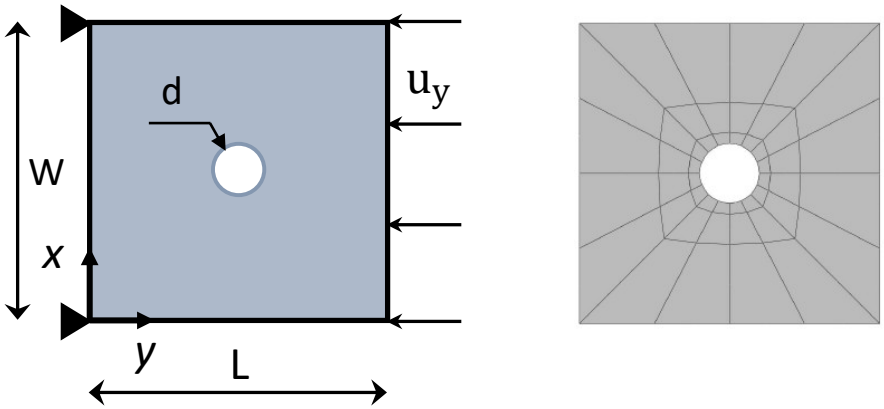

Figure 8: Geometry and boundary conditions of the open-hole specimen under compression loads. The FE mash has 48 Q9 elements

	L (mm)	W (mm)	d (mm)
Scale 1	32	32	6.35
Scale 2	64	64	12.70
Scale 3	128	128	25.40

Table 4: Dimensions of the open-hole specimen for three different scales

4.3 Open-hole compression test

The third numerical case refers to an open-hole specimen with a $[45/90/\text{-}45/0]_{4s}$ quasi-isotropic layup subjected to compression loads; it is based on the previous numerical works [23] and compared with the experimental tests made by Lee and Soutis in [42]. The geometry and boundary conditions are shown in Fig. 8, where dimensions W and L employed in this paper depend on the scale used and listed in Table 4. Table 5 lists the number of elements and DOF of models employed in this case.

The first set of results refers to Scale 1, and different CUF models are employed, with 48, 72, and 96 Q9 elements, and linear to cubic expansion functions. The post-peak softening

Model	Elements	DOF
	Scale 1	
CUF 48Q9-LE1	48 Q9 elements in-plane and 1 LE1 per ply	22176
CUF 48Q9-LE2	48 Q9 elements in-plane and 1 LE2 per ply	43680
CUF 48Q9-LE3	48 Q9 elements in-plane and 1 LE3 per ply	65184
CUF 72Q9-LE1	72 Q9 elements in-plane and 1 LE1 per ply	33264
CUF 96Q9-LE1	96 Q9 elements in-plane and 1 LE1 per ply	44352
MAT18 (LSDYNA)	1202 shell elements	NA
	Scale 2	
CUF 128Q9-LE1	128 Q9 elements in-plane and 1 LE1 per ply	57024
	Scale 3	
CUF 256Q9-LE1	256 Q9 elements in-plane and 1 LE1 per ply	114048

Table 5: Number of elements and DOF of models for the open-hole specimen

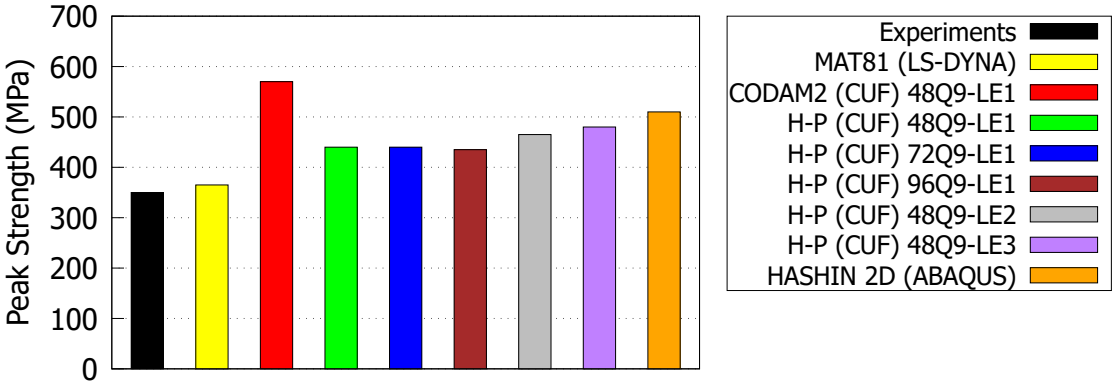

Figure 9: Comparison of peak strength values of the $[45/90/\text{-}45/0]_{4s}$ quasi-isotropic open-hole compression test for Scale 1 with different damage models, experiments and various CUF models with linear softening

is linear; see Fig. 9. The peak values are compared with experiments [42] and numerical cases obtained using the MAT18 damage model in LS-DYNA [23]. The figure shows also the numerical value obtained using ABAQUS with a damage model based on Hashin 2D failure criteria and 2D shell elements. Figure 10 shows the peak strength values obtained with various CUF models with linear-brittle post-peak softening and the H-P damage model; results are compared with experimental data, numerical ones based on MAT18 in LS-DYNA and previous CODAM2-CUF cases. The H-P CUF model's damage evolutions are shown in Fig. 11, for different values of displacements, -0.24 mm, -0.29 mm, and -0.31 mm; the results refer to the with 96 Q9 mesh and LE1. The final set of results refers to the peak failure strength obtained for three scales. The LE1 was used in all CUF results, and a linear brittle (Br-50) post-peak softening. In Fig. 12, the peak strength for H-P CUF models is compared with the CODAM2 CUF model with a linear brittle (Br-30) post-peak softening, experimental values and the MAT18 damage model in LS-DYNA [23]. The results suggest that:

1. The linear softening overestimates the peak stress of 20% compared to the experiment's value. Using H-P improves the results compared to CODAM2 and Hashin 2D from

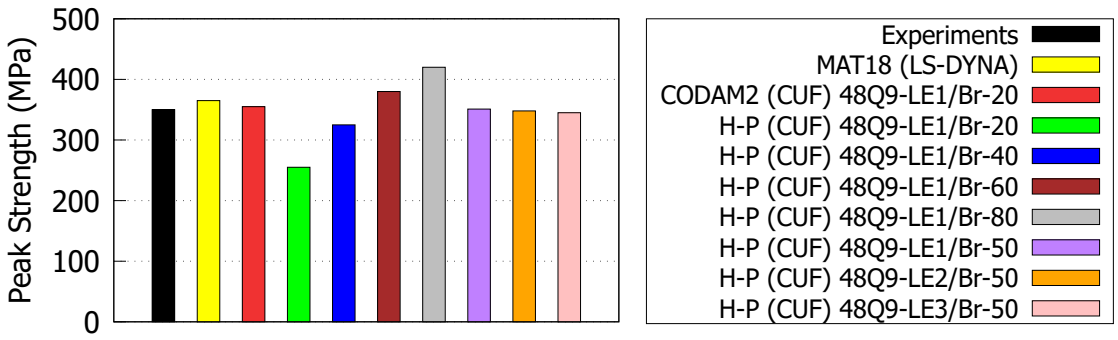

Figure 10: Comparison of peak strength values of the $[45/90/\text{-}45/0]_{4s}$ quasi-isotropic open-hole compression test for Ccale 1 with different post-peak softening

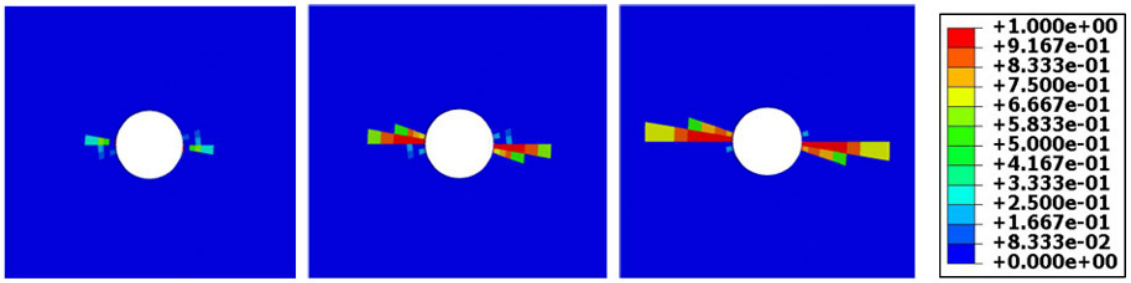

(a) Fiber damage evolution

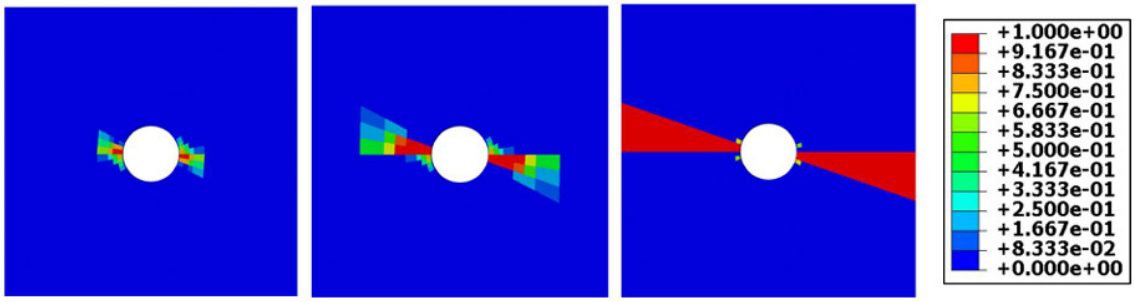

(b) Matrix damage evolution

Figure 11: Damage evolution of the $[45/90/\text{-}45/0]_{4s}$ quasi-isotropic open-hole compression test for a) fiber and b) matrix at -0.24 mm, -0.29 mm, and -0.31 mm; Scale 1

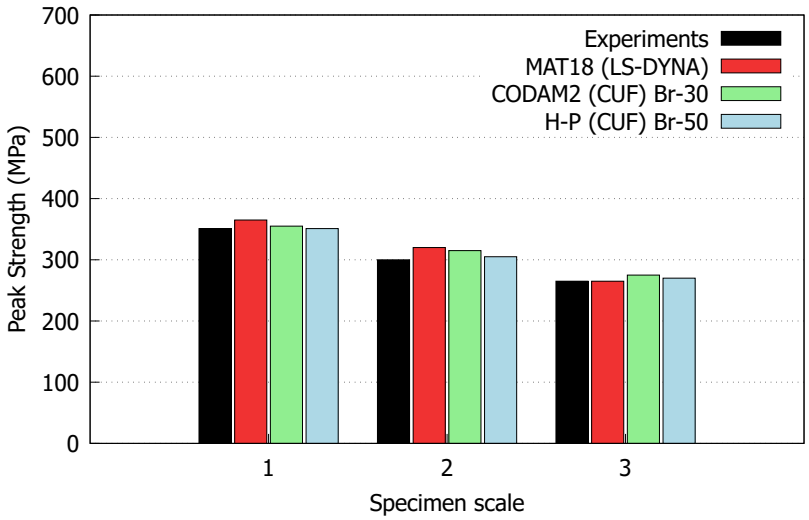

Figure 12: Comparison of peak strength values of the $[45/90/\text{-}45/0]_{4s}$ quasi-isotropic open-hole compression test for various scales

Abaqus as the peaks are 25% lower.

2. A 48 Q9 element mesh is enough to have converged results.

3. The linear-brittle softening models enhance the accuracy of peak values. The expansion variation from LE1 to LE3 has a negligible impact on the compressive peak value.

4. The H-P CUF approach with Br-50 is closer to the experimental results than MAT18 in LS-DYNA, exhibiting a reduced computational cost. The CUF model uses a 48 Q9 in-plane mesh, while the MAT18 model employs 1202 elements.

5 Conclusions

This work has presented results from combining Hashin 3D and Puck failure criteria (H-P) and refined 2D structural theories. The structural modeling is based on CUF and is layer-wise to retain the properties of each ply. Single-element tests, compact compression, and open-hole specimens were considered. Results were compared to other numerical approaches and experiments from the literature. The effect of various parameters on nonlinear equilibrium curves, peak force values, and damage progression was evaluated, including structural theories, FE meshes, and softening laws. The main conclusions are the following:

- Overall, the use of H-P has improved the accuracy compared to previous models such as the CODAM2.
- The use of linear-brittle softening curves allowed us to obtain a more precise prediction of the peak strength for the open-hole specimen subjected to compression. The linear softening was enough for the compact compression using H-P, while the linear brittle was necessary using CODAM2.
- Due to the in-plane nature of the cases considered, linear expansions of the ply displacement field are enough. The use of a layer-wise approach is mandatory as equivalent-single layer models provided poorer results.

Future investigation should concern multi-scale models to evaluate the propagation of damage at the microscopic level, the application of the global-local framework, and the development of a two-way coupling approach to account for local stiffness degradation.

Acknowledgments

This work was partially financed by the European Union - NextGenerationEU (National Sustainable Mobility Center CN00000023, Italian Ministry of University and Research Decree n. 1033 - 17/06/2022, Spoke 11 - Innovative Materials & Lightweighting). The opinions expressed are those of the authors only and should not be considered as representative of the European Union or the European Commission's official position. Neither the European Union nor the European Commission can be held responsible for them.

References

[1] P. D. Mangalgiri. Composite materials for aerospace applications. *Bulletin of Materials Science*, 22(3):657–664, May 1999.

[2] N. A. Fleck and B. Budiansky. *Compressive Failure of Fibre Composites Due to Microbuckling*, pages 235–273. Springer New York, 1991.

[3] K. Niu and R. Talreja. Modeling of compressive failure in fiber reinforced composites. *International Journal of Solids and Structures*, 37(17):2405–2428, April 2000.

[4] X. Chen, X. Sun, B. Wang, J. Gu, P. Zou, Y. Chai, and J. Yang. An improved longitudinal failure criterion for UD composites based on kinking model. *Mechanics of Advanced Materials and Structures*, 29(6):905–915, August 2020.

[5] W. Bai, L. He, and L. Peng. Study of the effect of void defects on the mechanical properties of fiber reinforced composites. *Mechanics of Advanced Materials and Structures*, pages 1–20, August 2024.

[6] S. Krishnappa and S. Gururaja. Numerical investigation of intrinsic competing damage mechanisms in unidirectional fiber reinforced polymer composites under compression. *Mechanics of Advanced Materials and Structures*, 31(27):9468–9485, November 2023.

[7] Q. Sun, G. Zhou, H. Guo, Z. Meng, Z. Chen, H. Liu, H. Kang, and X. Su. Failure mechanisms of cross-ply carbon fiber reinforced polymer laminates under longitudinal compression with experimental and computational analyses. *Composites Part B: Engineering*, 167:147–160, June 2019.

[8] E. V. Iarve, K. H. Hoos, Y. Nikishkov, and A. Makeev. Discrete damage modeling of static bearing failure in laminated composites. *Composites Part A: Applied Science and Manufacturing*, 108:30–40, May 2018.

[9] P. Ladeveze and E. Ledantec. Damage modelling of the elementary ply for laminated composites. *Composites Science and Technology*, 43(3):257–267, 1992.

[10] Z.C. Su, T.E. Tay, M. Ridha, and B.Y. Chen. Progressive damage modeling of open-hole composite laminates under compression. *Composite Structures*, 122:507–517, April 2015.

[11] A. Riccio, A. Sellitto, S. Saputo, A. Russo, M. Zarrelli, and V. Lopresto. Modelling the damage evolution in notched omega stiffened composite panels under compression. *Composites Part B: Engineering*, 126:60–71, October 2017.

[12] A. Rotem and Z. Hashin. Failure Modes of Angle Ply Laminates. *Journal of Composite Materials*, 9(2):191–206, April 1975.

[13] A. Puck and H. Schürmann. Failure analysis of FRP laminates by means of physically based phenomenological models. *Composites Science and Technology*, 62(12–13):1633–1662, September 2002.

[14] O. Hoffman. The Brittle Strength of Orthotropic Materials. *Journal of Composite Materials*, 1(2):200–206, April 1967.

[15] S. W. Tsai and E. M. Wu. A General Theory of Strength for Anisotropic Materials. *Journal of Composite Materials*, 5(1):58–80, January 1971.

[16] K. V. Williams, R. Vaziri, and A. Poursartip. A physically based continuum damage mechanics model for thin laminated composite structures. *International Journal of Solids and Structures*, 40(9):2267–2300, May 2003.

[17] A. Forghani, N. Zobeiry, A. Poursartip, and R. Vaziri. A structural modelling framework for prediction of damage development and failure of composite laminates. *Journal of Composite Materials*, 47(20–21):2553–2573, January 2013.

[18] J. Reiner, T. Feser, D. Schueler, M. Waimer, and R. Vaziri. Comparison of two progressive damage models for studying the notched behavior of composite laminates under tension. *Composite Structures*, 207:385–396, January 2019.

[19] M. Shahbazi. *An efficient virtual testing framework to simulate the progression of damage in notched composite laminates*. PhD thesis, 2017.

[20] X.C. Sun and S.R. Hallett. Barely visible impact damage in scaled composite laminates: Experiments and numerical simulations. *International Journal of Impact Engineering*, 109:178–195, November 2017.

[21] M. Akterskaia, E. Jansen, S. R. Hallett, P. M. Weaver, and R. Rolfes. Progressive Failure Analysis Using Global-Local Coupling Including Intralaminar Failure and Debonding. *AIAA Journal*, 57(7):3078–3089, July 2019.

[22] M.H. Nagaraj, J. Reiner, R. Vaziri, E. Carrera, and M. Petrolo. Progressive damage analysis of composite structures using higher-order layer-wise elements. *Composites Part B: Engineering*, 190:107921, June 2020.

[23] M.H. Nagaraj, J. Reiner, R. Vaziri, E. Carrera, and M. Petrolo. Compressive damage modeling of fiber-reinforced composite laminates using 2D higher-order layer-wise models. *Composites Part B: Engineering*, 215:108753, June 2021.

[24] Y. Zhang, W. Van Paepegem, and W. De Corte. An Enhanced Progressive Damage Model for Laminated Fiber-Reinforced Composites Using the 3D Hashin Failure Criterion: A Multi-Level Analysis and Validation. *Materials*, 17(21):5176, October 2024.

[25] L. Bek, R. Kottner, and V. Laš. Material model for simulation of progressive damage of composite materials using 3D Puck failure criterion. *Composite Structures*, 259:113435, March 2021.

[26] A. Puck and H. Schürmann. *Failure analysis of FRP laminates by means of physically based phenomenological models*, pages 832–876. Elsevier, 2004.

[27] C. Dogan, M. O. Kaman, S. Erdem, and M. Albayrak. Comparison of Hashin and Puck criterions for failure behavior of pin loaded composite plates. *Materialwissenschaft und Werkstofftechnik*, 55(3):314–329, March 2024.

[28] C. Davila, N. Jaunky, and S. Goswami. Failure Criteria for FRP Laminates in Plane Stress. In *44th AIAA/ASME/ASCE/AHS/ASC Structures, Structural Dynamics, and Materials Conference*. American Institute of Aeronautics and Astronautics, April 2003.

[29] E. Carrera. Theories and Finite Elements for Multilayered Plates and Shells:A Unified compact formulation with numerical assessment and benchmarking. *Archives of Computational Methods in Engineering*, 10(3):215–296, September 2003.

[30] I. Kaleel, M. Petrolo, and E. Carrera. Elastoplastic and progressive failure analysis of fiber-reinforced composites via an efficient nonlinear microscale model. *Aerotecnica Missili & Spazio*, 97(2):103–110, April 2018.

[31] M. Petrolo and P. Iannotti. Best Theory Diagrams for Laminated Composite Shells Based on Failure Indexes. *Aerotecnica Missili & Spazio*, 102(3):199–218, June 2023.

[32] E. Carrera and V.V. Zozulya. Carrera Unified Formulation (CUF) for the composite plates and shells of revolution. Layer-wise models. *Composite Structures*, 334:117936, April 2024.

[33] I. Lapczyk and J. A. Hurtado. Progressive damage modeling in fiber-reinforced materials. *Composites Part A: Applied Science and Manufacturing*, 38(11):2333–2341, November 2007.

[34] X. Li, D. Ma, H. Liu, W. Tan, X. Gong, C. Zhang, and Y. Li. Assessment of failure criteria and damage evolution methods for composite laminates under low-velocity impact. *Composite Structures*, 207:727–739, January 2019.

[35] M.V. Donadon, L. Iannucci, B.G. Falzon, J.M. Hodgkinson, and S.F.M. de Almeida. A progressive failure model for composite laminates subjected to low velocity impact damage. *Computers &; Structures*, 86(11–12):1232–1252, June 2008.

[36] M. Rezasefat, D. Badel Torres, A. Gonzalez-Jimenez, M. Giglio, and A. Manes. A fast fracture plane orientation search algorithm for Puck's 3D IFF criterion for UD composites. *Materials Today Communications*, 28:102700, September 2021.

[37] A. Matzenmiller, J. Lubliner, and R.L. Taylor. A constitutive model for anisotropic damage in fiber-composites. *Mechanics of Materials*, 20(2):125–152, April 1995.

[38] N. Zobeiry. *Extracting the strain-softening response of composites using full-field displacement measurement*. PhD thesis, 2010.

[39] J. Reiner, N. Zobeiry, and R. Vaziri. A stacked sublaminate-based damage-plasticity model for simulating progressive damage in composite laminates under impact loading. *Thin-Walled Structures*, 156:107009, November 2020.

[40] T. Reiner, J.and Feser, M. Waimer, A. Poursartip, H. Voggenreiter, and R. Vaziri. Axial crush simulation of composites using continuum damage mechanics: FE software and material model independent considerations. *Composites Part B: Engineering*, 225:109284, November 2021.

[41] N. Zobeiry, R. Vaziri, and A. Poursartip. Characterization of strain-softening behavior and failure mechanisms of composites under tension and compression. *Composites Part A: Applied Science and Manufacturing*, 68:29–41, January 2015.

[42] J. Lee and C. Soutis. Measuring the notched compressive strength of composite laminates: Specimen size effects. *Composites Science and Technology*, 68(12):2359–2366, September 2008.